International Journal of Neural Systems

LATERAL INHIBITION ORGANIZES BETA ATTENTIONAL MODULATION IN THE PRIMARY VISUAL CORTEX

ELŻBIETA GAJEWSKA-DENDEK
Department of Biomedical Physics, Institute of Experimental Physics, University of Warsaw
5 Pasteur St, 02-093 Warsaw, Poland

ANDRZEJ WRÓBEL
Department of Neurophysiology, Nencki Institute of Experimental Biology
3 Pasteur St, 02-093 Warsaw, Poland

MAREK BEKISZ
Department of Neurophysiology, Nencki Institute of Experimental Biology
3 Pasteur St, 02-093 Warsaw, Poland

PIOTR SUFFCZYNSKI
Department of Biomedical Physics, Institute of Experimental Physics, University of Warsaw
5 Pasteur St, 02-093 Warsaw, Poland
E-mail: Piotr.Suffczynski@fuw.edu.pl

We have previously shown that during top-down attentional modulation (stimulus expectation) correlations of the beta signals across the visual cortex were uniform, while during bottom-up attentional processing (visual stimulation) their values were heterogeneous. These different patterns of attentional beta modulation may be caused by feed-forward lateral inhibitory interactions in the visual cortex, activated solely during stimulus processing. To test this hypothesis we developed a large-scale computational model of the cortical network. We first identified the parameter range needed to support beta rhythm generation, and next, simulated the different activity states corresponding to experimental paradigms. The model matched our experimental data in terms of spatial organization of beta correlations during different attentional states and provided a computational confirmation of the hypothesis that the paradigm-specific beta activation spatial maps depend on the lateral inhibitory mechanism. The model also generated testable predictions that cross-correlation values depend on that distance between the activated columns and on their spatial position with respect to the location of the sensory inputs from the thalamus.

Keywords: beta frequency band, attention, visual cortex, computational model.

1. Introduction

There is accumulating evidence that beta range oscillations, generally defined as 14–30 Hz, are linked to purposeful mental activity. Beta activity has been primarily associated with attention processes and increased vigilance[1-7] but has also been implicated in motor behavior[8-10] sensorimotor decision making,[11-13] language processing,[14] learning,[15] and the maintenance of the current sensorimotor or cognitive state.[16] These different functions are accompanied by power changes in beta signals within local circuits and the modulation of network interactions occurring within the beta frequency range.[17, 18] Recently, we investigated the spatiotemporal patterns of beta activity, in a sub-range of 16-24 Hz, using local field potential (LFP) imaging,[19] in the primary visual cortex of cats that performed bottom-up and top-down attentional tasks. We showed that during both tasks the beta power increased but its spatiotemporal organization across cortical sites varied distinctively. A stimulus-driven bottom-up task produced a spatially heterogeneous beta activity correlation pattern while an anticipatory top-down task led to spatially homogenous beta correlations. We hypothesized that during bottom-up attention tasks, the columns of the primary cortex, which are involved in

processing of a stimulus, exhibited strong beta activity, while neighboring columns, which are suppressed by lateral inhibitory mechanisms, exhibited weaker beta signals. Activated columns could account for higher inter-column correlations, while pairs of suppressed (or activated-suppressed) columns presumably led to lower correlations. On the contrary, in the top-down attentional paradigm, columns of the primary cortical areas are assumed to be activated more uniformly by top-down diffuse beta modulatory signals, leading to similar inter-column correlation values. The aim of the present research is to complete our previous study[19] using computer simulations that are set up to test the proposed neurophysiological mechanism. Accordingly, we developed a large-scale computational model of the cortical network consisting of Hodgkin-Huxley neurons and the basic connectivity of the primary visual cortex. Using the model, we first investigated the conditions that are suitable for the emergence of beta band rhythms. Next, we simulated the conditions for bottom-up and top-down attentional states and the corresponding spatial patterns of their beta correlations. We have shown that sensory input together with the lateral inhibitory mechanism might account for the heterogeneous pattern of the spatial beta correlations, while anticipatory activation from the higher order cortical centers might result in spatially homogenous excitation. Furthermore, the model generates testable predictions that distance between the activated columns and their spatial position with respect to location of the sensory inputs from the thalamus are main factors shaping beta cross-correlations between the cortical recording sites.

2. Experimental data

The LFP signals were recorded from the primary visual cortex of seven cats. The animals were trained using two attentional paradigms: stimulus-driven and anticipatory (see Ref. 19 for details). During the experiments the animals were placed in an experimental box and performed visual and auditory spatial discrimination tasks in a randomly intermingled order. In the stimulus driven (bottom-up) paradigm, a moving light bar or a loudspeaker producing white noise were produced behind a front wall with two feeding doors. The 12–20 trials (each lasting 10–20 s) for each modality were executed in daily sessions. The animal was required to remember on which side (left or right) of the box the stimulus was turned off in order to be allowed to obtain a food reward from behind the matching door after a 2 s delay. In the anticipatory (top-down) paradigm the animals received a 1 s cue: light flash or a white noise auditory signal delivered in front of the box. After 8–14 s the 1 s visual or auditory target stimulus was delivered at one of the doors, indicating the placement of a food reward, to be obtained also with 2 s delay. The learning procedure ended when the animals performed the tasks with 90% accuracy. The active beta range in cats' attention experiments, 16–24 Hz, was filtered out from the LFP signals recorded from two to four chronic electrodes implanted in the primary visual cortex. The correlations between the filtered beta signals recorded during stimulus presentation (in the bottom-up paradigm) or anticipation (in the top-down paradigm) in attentional visual trials were referenced to beta correlations during similar periods in auditory trials.

3. Computational model

3.1. *Neuron types*

Our neuronal network consisted of single compartment excitatory (E) and inhibitory (I) cells modeled with extended Hodgkin-Huxley dynamics. Excitatory neurons corresponded to regular spiking cortical cells while the firing of inhibitory neurons simulated fast spiking cortical interneurons. The E neurons exhibited firing adaptation at the beginning of the injected depolarizing current, while the I neurons were characterized by a higher firing rate and a lack of adaptation in response to the injected depolarizing current. The model equations and parameters for the two different types of cells (regular spiking and fast spiking) were based on the earlier modeling study,[20] where single cell behavior was presented.

3.2. *Network architecture*

The columnar architecture of the cortex is characterized by cortical patches, which are aggregations of cells up to within 500 μm diameter.[21, 22] Accordingly, in the model we grouped the cells into 16 columns arranged in a two-dimensional matrix, with the inter-columnar centers spaced 1 mm apart (double the 500 μm column diameter) (Fig. 1A). The individual columns consisted of single layer neuronal networks with both E and I cells, the excitatory cells being four times more

numerous than inhibitory. Such a proportion of E and I cortical neurons roughly corresponds to histological data[21] and is commonly used in computational models of the cortex.[23, 24] Nevertheless, such an approach is a significant simplification, as different neuron classes of both excitatory and inhibitory cells with different biophysical properties are known to exist in the cortex.[25, 26]

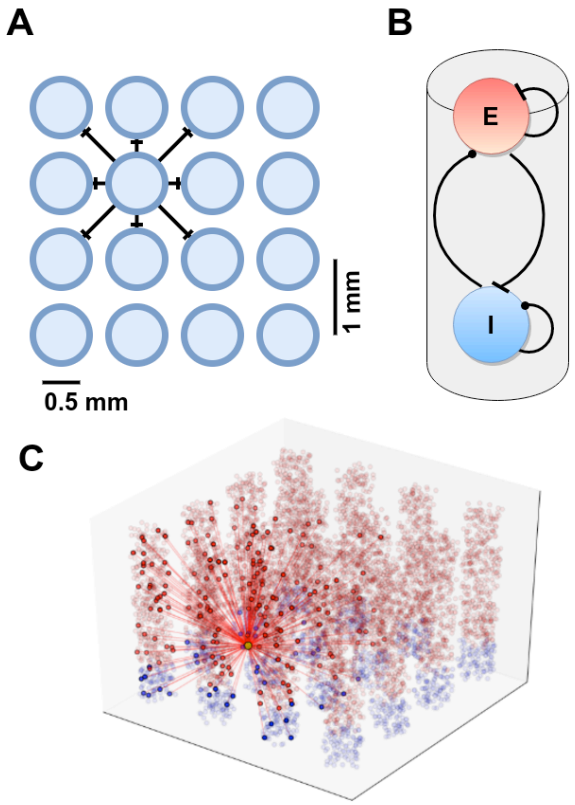

Fig. 1. A schematic view of the connections between columns (A) and within a column (B), of the model. A: the network consists of 16 columns arranged in a 4×4 matrix with a 1 mm inter-column distance (center to center) and a column diameter of 0.5 mm. The connections between the columns are only excitatory: E→E, E→I (E-Excitatory, I-Inhibitory). They are created exclusively between neighboring columns. Exemplary outgoing connections from a single column are shown in the diagram. B: each column consists of excitatory and inhibitory neurons, with all possible connection types within and between neuron types: E→E, E→I, I→E and I→I. Excitatory connections are marked with bars, inhibitory ones, with circles. C: A schematic visualization of the network composed of 16 columns with excitatory (red) and inhibitory (blue) populations. For the purposes of image clarity only convergent connections are shown for randomly picked single excitatory neuron, and the depth of the layer was extended for better readability.

In order to create a model that matches real cortical wiring we began with experimental data on neuron and synapse quantities in the primary visual cortex of cats. Next, we estimated the total number of neurons and connections that corresponded to a single cortical column. In our calculations we treated all cortical layers as one ensemble and summed number of connections across all layers. In this way we got simplified pattern of connectivity as if the density of different types of cells (E or I) and synaptic connections would be uniform within a cortical column. Then, we scaled down the number of neurons and connections. Finally, we computed the number of convergent connections that were assigned to each neuron in the model.

In cats the total number of neurons for all six cortical layers in area V1 is about 34×10^6 neurons per 339 mm^2 area of cortical surface.[27] Accordingly, the neuron density in a cat's primary visual cortex is approximately 1×10^5 per 1 mm^2, with a density 0.8×10^5 per 1 mm^2 for E cells and 0.2×10^5 per 1 mm^2 for I cells. Assuming that a column's area can be approximated by the area of a circle with a diameter of 500 μm (~0.2 mm^2), a single column would contain 16,000 E cells and 4,000 I cells. In order to meet available computational power we scaled down the number of neurons using the ratio ξ=1/40. As a result, a single cortical column in the model contained 400 excitatory and 100 inhibitory neurons while the whole network of 16 cortical columns contained 6,400 excitatory and 1,600 inhibitory neurons.

3.3. *Synaptic connections*

According to experimental data,[27] the number of synapses connecting different classes of neurons, that is, E→E, E→I, I→E and I→I, in all layers of a cat's area 17 are 13.6×10^{10}, 2.1×10^{10}, 2.4×10^{10} and 0.4×10^{10}, respectively. Additionally, according to Ref. 28, the majority of excitatory connections are long-range, as 74% of synapses are made by neurons that are located more than 500 μm away. In order to estimate the number of synapses within a single cortical column, the connection numbers were scaled down by a ratio of the area of the column divided by the area of V1, which resulted in 78.8×10^6 E→E synapses (out of which 19.7×10^6 were assigned as local), 12.2×10^6 E→I (out of which 3×10^6 were local), 13.9×10^6 I→E, and 2.3×10^6 I→I.

Within a single column we modeled all the possible types of connections: E→E, E→I, I→E and I→I (Fig. 1B). The excitatory connections within the column consisted of only 26% of all excitatory synapses according to the experimental data.[28] The connections between different columns were only excitatory. For the sake of simplicity we decided to neglect the inhibitory connections between columns as inhibitory connections are most commonly found to be local. In the analyzed brain tissue, only 34% of the total number of inhibitory synapses originate from neurons that are located more than 250 μm away, and the number falls below 20% for the neurons located more than 500 μm away.[28] The connection numbers were scaled down by a factor of ξ^2, resulting in 31 excitatory and 22 inhibitory connections converging on each E cell, and 20 excitatory and 15 inhibitory connections converging on I cell within-column. The inter-columnar connections (Fig. 1A) were comprised of E→E and E→I connections, which are assumed to exist only between adjacent columns. As a result of scaling by a factor of ξ^2, each of the E and I neurons received respectively 92 and 59 excitatory inputs originating in neighboring columns.

The synaptic connections included fast ionotropic excitatory AMPA and inhibitory $GABA_A$ type receptors. Post-synaptic currents were described by a double exponential function. The rise and decay times for excitatory postsynaptic currents (EPSC) were 0.5 ms and 5 ms, and for inhibitory postsynaptic currents (IPSC), 0.5 ms and 2 ms. The value of synaptic current was proportional to synaptic weight w, time-dependent conductance g, and the difference between cell membrane potential V and the reversal potential E_{syn}; obeying the equation

$$I_{syn}(t) = w \cdot g(t) \cdot (V(t) - E_{syn}). \qquad (1)$$

The relative connection weights were assigned to 3.5, 14, -70, -70 for E→E, E→I, I→E and I→I, respectively. The weights of the inhibitory synapses were higher since these synapses are predominantly located closer to the cell soma.[29, 30] For the chosen weights and conductances the EPSP amplitudes (for E→E connections) were +0.3 mV, and the IPSP amplitudes (for I→E) were -1.5 mV, in response to a single presynaptic spike. The neuronal delays between two coupled neurons were calculated assuming an axonal propagation speed equal to 0.8 mm/ms,[31] and a synaptic delay equal to 0.5 ms.[32] For these values, delays for the short-range connections were within 0.5–1.5 ms range and for the long-range connections within 0.9–2.0 ms range.

3.4. *Inputs*

We equipped the modeled cortical neurons with three kinds of inputs; these represented the following: the activation from the higher order cortical regions (I_C and I_{comm}), the background input from the thalamus (I_B), and a specific visual input (I_S) from the thalamus. The inputs are described below and their arrangement is shown in

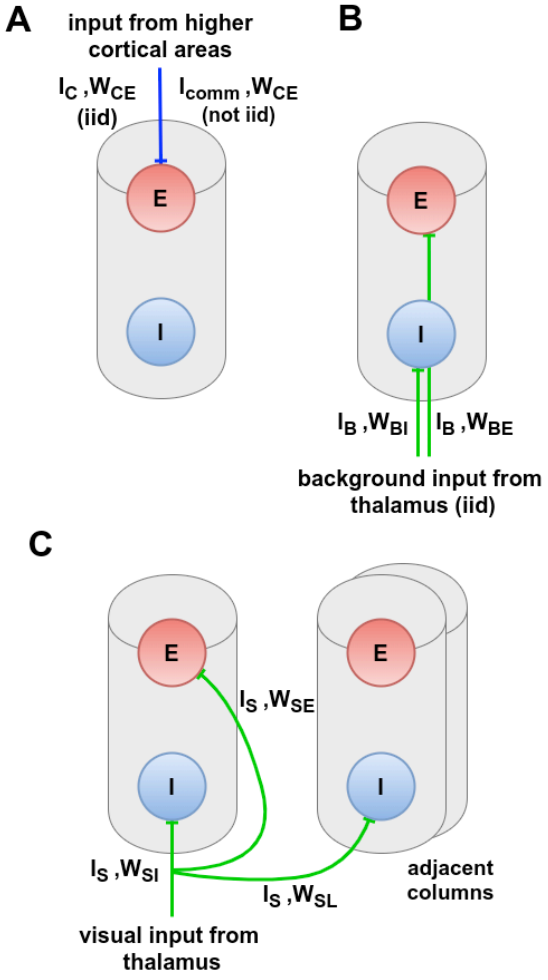

Fig. 2. A schematic representation of the external inputs. A: Cortical and common inputs, I_C and I_{comm}, from higher cortical areas to excitatory cells in V1 (blue line). B: Background input I_B from the thalamus arriving at both excitatory and inhibitory cells (green lines). C: Specific visual input, I_S, from the thalamus reaches both populations of excitatory and inhibitory cells from the retinotopically targeted column and inhibitory interneurons of the adjacent columns (green lines). W_{CE}, W_{BI}, W_{BE}, W_{SE}, W_{SI} and W_{SL} denote the respective connection weights associated with each type of input as described in the text. E - excitatory, I - inhibitory.

Fig. 2.

Cortical input

The cortical input, $I_{C,}$, was modeled as independent and identically distributed ('iid') Poisson spike trains arriving at each of the excitatory neurons (Fig. 2A). It had a synaptic weight W_{CE} equal to 3.7, and was adjusted such that, together with the selected value of $I_{C,}$ the neurons fired at low firing rates (<10 Hz) and the network produced beta oscillations seen also in the experimentally recorded LFP signal. The inputs to cortical neurons from the higher order cortical areas can be partly correlated, for example, due to the divergence of incoming cortico-cortical connections (see Ref. 33, Chapter 34). Such correlated inputs may have a strong impact on the measured correlations between LFP signals recorded at two cortical sites.[34] To account for the relatively high spatial correlations in the experimental data, it was necessary to introduce a fraction of cortical input, consisting of the same Poisson spike train, arriving at each excitatory neuron. This so-called common input I_{comm} had the same weight W_{CE} as the I_C input.

Thalamic background input

The thalamic background input, $I_{B,}$ was also modeled as 'iid' feeding each of the E and I neurons (Fig. 2B). The I_B input was given synaptic weights W_{BE} for excitatory neurons and W_{BI} for inhibitory neurons, equal to 2.0 and 1.0, respectively. The thalamic connections to excitatory neurons were stronger than to inhibitory ones based on anatomical data[27] and were similar to other thalamocortical models.[35]

Specific visual input

The specific visual input, $I_{S,}$ provided activation for both excitatory and inhibitory neurons in the target columns, as well as the inhibitory populations of the adjacent columns (Fig. 2C). This type of connectivity pattern is responsible for the lateral inhibition mechanism at the cortical level.[36] I_S was modeled as a single realization of the Poisson spike train. The I_S input was given synaptic weights W_{SE} for excitatory neurons and W_{SI} for inhibitory neurons, equal to 2.0 and 1.0, respectively. The weight of the specific-lateral connection, that is, of the I_S input arriving at inhibitory cells in the adjacent columns was set to $W_{SL} = 0.4$. This value appeared to be optimal for modulating beta power in the surround, while preserving population activity. Higher weights resulted in a significant reduction in spiking in adjacent populations, while lower weights produced too subtle effect.

It should be noted that in general the thalamus receives strong cortical feedback. In our model we didn't include such reciprocal connections between the thalamus and cortex. Instead we model stationary states of the network, in which feedback has stationary values that are accounted for by appropriate setting of the inputs.

3.5. *Definition of states*

In order to be able to compare the modeling results with the experimental data, we introduced into the model three states that corresponded to different experimental conditions. The reference (Ref) state of the model corresponded to the experimental auditory task. Under these conditions we assumed a moderate strength of external cortical input to the visual cortex, background thalamic input at its reference value and the absence of a specific thalamic visual input. The parameter settings for this state were as follows: $I_C = 300$ Hz, $I_B = 210$ Hz and $I_S = 0$. For these parameter values we observed weaker beta band activity in the modeled LFP signals (see paragraph 3.6 below). The anticipatory attention (Ant) state of the model corresponded to the experimental situation in which a cat was attentively staring at the front wall of the cage waiting for the visual stimulus to appear, yet without any stimulus present. Accordingly, we modeled this state using an increased external cortical input, the background thalamic input at its reference value, and an absence of specific thalamic visual input. For this state the parameters were as follows: $I_C = 320$ Hz, $I_B = 210$ Hz and $I_S = 0$. With these settings a clear peak in the beta range was observed in the spectrum of modeled LFP signal. The stimulus-driven attention (SD) state referred to the experimental situation in which a cat actively fixated and followed the visual stimulus. In this state the cortical and background thalamic inputs were the same as for the anticipatory attention state, and thalamic sensory input was added to the target columns. Here we present the results of the sensory input arriving at two central columns (out of 16 total). This shows most clearly the inhibitory surround effect in the 10 neighboring columns. This effect diminished but was

still present when sensory information was passed to one, or more than two columns. Parameter settings for the SD state were as follows: I_C = 320 Hz, I_B = 210 Hz and I_S = 420 Hz. Each of the stimulated columns was fed by an individual Poisson spike train. For these parameter values we observed a strong beta signal in the target columns and weaker beta band activity in the neighboring ones. In all three attentional states described above, the common cortical input, I_{comm}, had a mean rate of 80 Hz (25% of the I_C value in the Ant and SD states). As the I_{comm} was identical in all simulated paradigms, it could not account for the differences in spatial correlations produced by the model in different states.

3.6. *LFP*

It is generally assumed that local field potential (LFP) activity mainly reflects synchronized postsynaptic potentials (e.g., Ref. 37). Furthermore, in real neurons, synaptic actions generate a paired sink and source for the current, which can be approximated by an electric dipole.[38] The largest contributions to LFP come from pyramidal cells due to the large spatial separation between their current sinks and sources, anatomical order, and temporal synchrony.[39] Accordingly, the local field potentials were modeled as the sum of both the excitatory and inhibitory synaptic currents for all the excitatory neurons in a single column. Additionally, in order to account for the dipolar distribution, the synaptic currents were scaled using the function $\sim 1/r^2$, where r corresponds to the distance between the synaptic current and point of measurement. The simulated LFP electrodes had a diameter 100 μm and were located in the center of each column, 50 μm above the neuronal layer. As a consequence, 16 LFP signals were obtained from the whole network.

3.7. *Computational environment*

The model was simulated by means of the PyNEST 2.2 package[40] and its extension, which included a custom-made implementation of specific cell types: regular and fast spiking neurons. The Euler forward method was used for the numerical integration routine with a time step of 0.01 ms. Typical 11 s simulation of a 4 × 4 column model took four hours to run on a 2.0–2.8 GHz AMD or Intel processor. All post processing was performed in a Linux system with Python 2.7 and version 0.13 of Scipy.

3.8. *Data analysis*

For the purposes of signal analysis, the membrane potentials or synaptic currents were recorded at a 1 kHz sampling rate. In order to estimate power spectral density, the Welch method was applied using a Hanning window with a length of 512 samples. Action potentials were detected based on neuron membrane potential with the threshold set to 0 mV. The instantaneous population firing rate is the time series that represents the number of spikes of all neurons within the population, fired within 2.5 ms time bins (see example in Fig. 5B).

In order to reduce the high frequency component, simulated LFPs were digitally filtered using a fifth order Chebyshev type II low-pass filter, with no phase shift

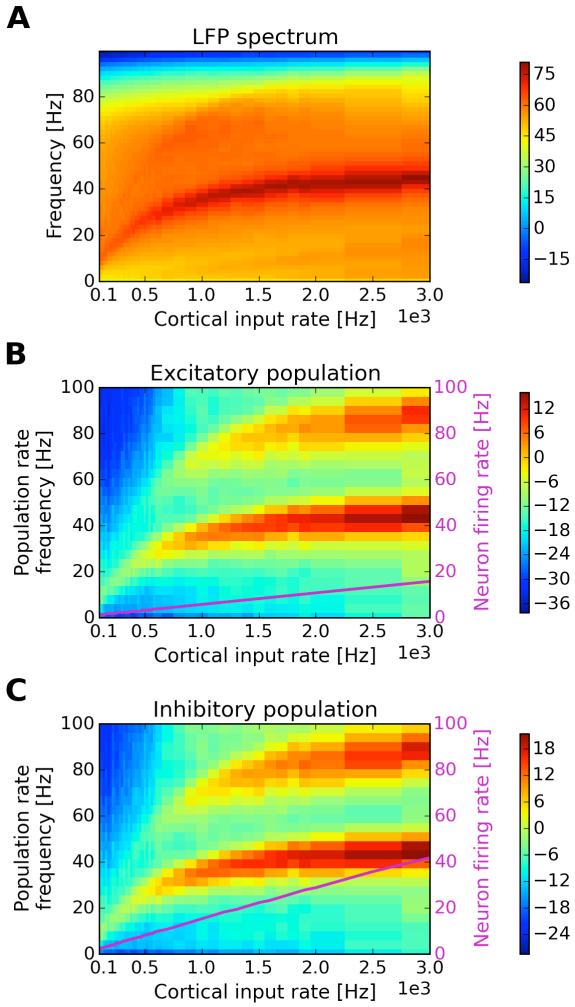

Fig. 3. A: the dependency of a power spectrum of LFP on mean external input strength. B, C: the dependency of power spectrum of the time series of Excitatory and Inhibitory population firing rates on mean strength of the top-down input. Mean firing rates for exemplary E and I neurons are marked with magenta on the respective plots. Colorbars represent spectral power values of the LFP signal in dB.

and a minimal attenuation of 30 dB for frequencies above the 94 Hz frequency range. For correlation analysis the signals were additionally band-pass filtered without phase shift, by means of fourth order Butterworth filter with half-amplitude cut-off frequencies of 16 Hz and 24 Hz.

The correlation analysis was analogous to that in the experimental work,[19] that is, simulated LFPs were first filtered in the beta range (16–24 Hz) and, subsequently, the unbiased cross-correlation function was computed. Finally, the maximum for the cross-correlation function within the limited time lag around zero (-1 s, +1 s) was chosen as the correlation value. This measure is unfortunately sensitive to the duration of the signals: shorter signals tend to give higher values than longer ones with the same properties. In our work we addressed this problem by setting the time of all simulations to 10 s and omitting the first 2 s from the computations to remove the possible influence by the initial conditions. Correlations were computed for all possible pairs for the 16 signals and the resulting 120 values were presented on scatter plots or in boxplots for comparison with in-vivo correlation measurements between different electrode pairs.

4. Results

4.1. *The influence of a noise mean rate on network frequency*

We first investigated how the LFP oscillation peak frequency in a single column depended on the cortical input rate. We performed series of simulations and varied the mean rate of the I_C input in the range 100 Hz – 3 kHz in steps of 20 Hz, 100 Hz, and 500 Hz, as we used more dense representation for lower input rates. During the analysis other inputs were at their reference values, i.e., I_B = 210 Hz and I_S = 0. The dependence of the LFP power spectrum on the mean input noise rate is presented in Fig. 3A, while Fig. 3B and C show the impact of input strength on the power spectrum of the instantaneous population firing rate. Additionally, the mean firing rates of individual E and I neurons are shown in Fig. 3B and C using a magenta line. The LFP oscillations emerge from alpha frequencies (around 10 Hz) and increase in frequency through the beta range (around 20 Hz) up to a slow saturation around the gamma frequencies (40 Hz; Fig. 3A). Figure 3B and C reveals that the frequency of LFP activity corresponded very accurately to the frequency of the instantaneous firing rates of both populations of cells (E and I). Additionally, due to nonsinusoidal shape of the instantaneous firing rate signal, second harmonic component is also present in Fig. 3B and C. At same time, individual neurons' firing rates were rather independent on the LFP frequency. Single cell frequencies of both cell types increase linearly with the external input strength, but they don't correspond to the population rhythm.

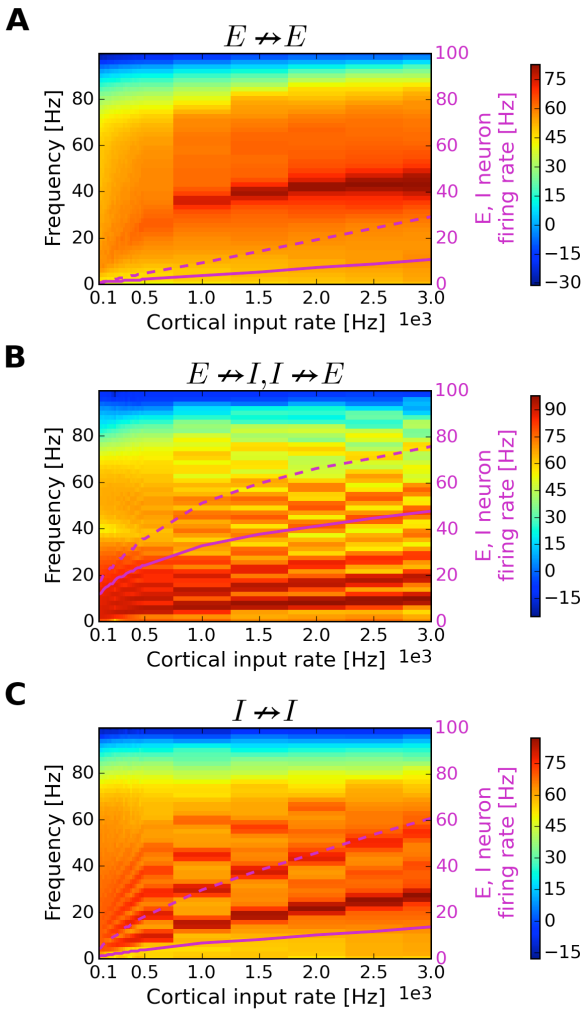

Fig. 4. The dependency of the LFP's power spectrum on the mean external input strength with, (A) excitatory to excitatory connections removed; (B) reciprocal connections removed; and (C) inhibitory to inhibitory connections removed. On the same plots the single E (solid line) and I (dashed line) neuron mean firing rate is marked with magenta. The color bar represents spectral power values in dB, of the LFP signal. E-excitatory, I – inhibitory.

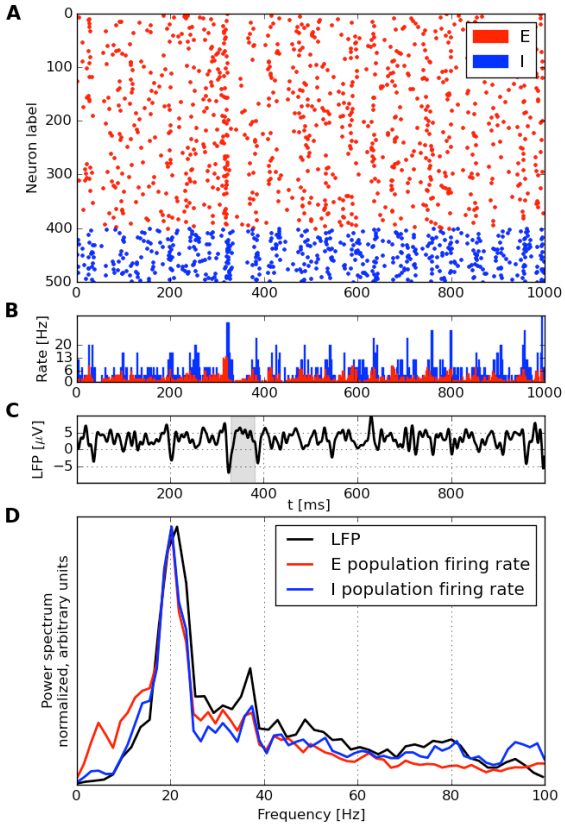

Fig. 5. A: Raster-plot showing spikes of inhibitory (I, in blue) and excitatory neurons (E, in red) in the single column of the model. B: Instantaneous firing rates of both populations computed in 2.5 ms time bins. Oscillations around 20 Hz are visible at the population firing level. The increase in the excitatory firing rate (red) precedes the increase in the inhibitory spike rate (blue). C. Simulated LFP signal. Oscillations at the frequency of 20 Hz are clearly visible in the LFP, with the most evident beta cycle marked in grey. D: The power spectrum of the LFP signal and of the time series of excitatory and inhibitory instantaneous population firing rates. Spectra were normalized to have the same amplitude in order to visualize the spectral peaks. The spectra of all three signals exhibited their most prominent peak in the beta frequency range (~ 20 Hz).

4.2. *The role of connection types between populations*

In order to determine which connection types were crucial for generating synchronized oscillations in the network we modified the network by selectively disabling individual connection types and then observed the reduced network behavior for a range of external input strength values. Removing excitatory to excitatory connections (Fig. 4A) did not affect the frequency of network oscillation, which remained in the beta-gamma range. Removing excitatory to inhibitory connections or removing inhibitory to excitatory connections (Fig. 4B) led to the deactivation of inhibitory cells and the independent activity of excitatory neurons. The oscillations that emerged consisted of highly synchronous bursts generated by the E neurons at around 10 Hz frequency. The highly synchronized activity produced a regular oscillation in the LFP signal, which was characterized by multiple harmonics in the power spectrum, as can be seen in Fig. 4B. Removing inhibitory to inhibitory connections (Fig. 4C) slowed down the oscillation in comparison to the intact network. The excitatory neurons fired at similar firing rates below 20 Hz, while disinhibited inhibitory neurons fired faster, reaching 60 Hz for maximal external drive. Multiple harmonics in the power spectrum, seen in Fig. 4B and C, originated most likely due to the fact that analyzed signals had complex waveform that couldn't be represented by a single sine wave.

The simulations described above suggest that beta/gamma oscillations may be dependent on the reciprocal interactions between E and I neurons. However, in simulations without the E→I connections, the interneurons did not receive excitatory input and therefore remained inactive, which in turn led to the abolition of beta/gamma oscillations. To verify whether the lack of beta/gamma activity was due to the lack of the overall inhibition of the E network or specifically due to the lack of reciprocal interactions between excitatory and inhibitory neurons, we performed an additional simulation without the E→I connections, but with the activity of I neurons triggered by external Poisson spike trains applied to every I neuron. The external input to I neurons was adjusted in order to produce a firing rate at 5.5 Hz, the same as observed during the beta activity in the intact network. Under these conditions the network generated synchronized bursts of activity that resembled the activity generated in the purely excitatory network. This allowed us to conclude that the recurrent interactions between E and I cells were crucial for generating beta/gamma activity in the model.

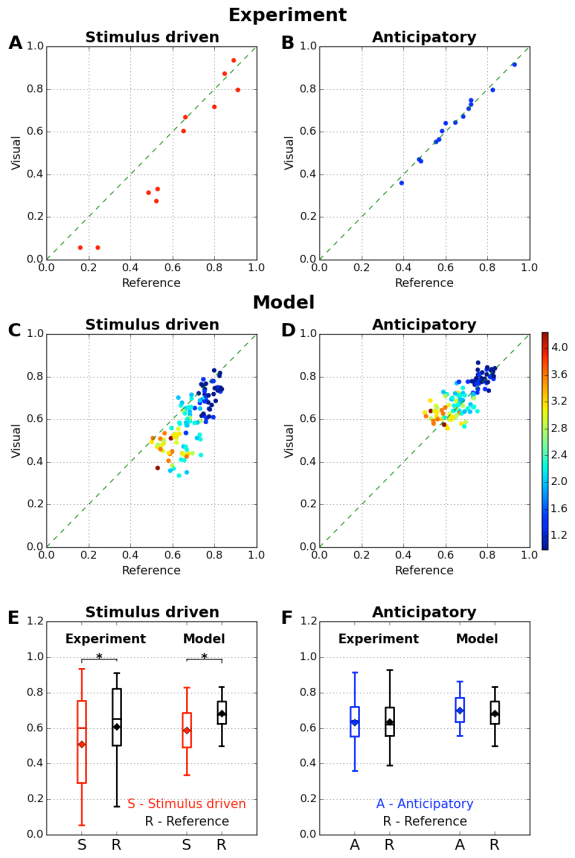

Fig. 6. The comparison of the cross-correlation results *in vivo* and in the model. A and B. Experimental scatterplots of the cross-correlation values for individual pairs of cortical recording sites in both attentional states: stimulus driven (A, red) and anticipatory (B, blue). Correlation values during attentional states in the visual paradigms are plotted against the correlation values for the reference (auditory) state. In the stimulus-driven paradigm the signals from pairs of recording sites with lower correlations in the reference state (0.3–0.6) exhibited significant decorrelations in the attentional state, while pairs with higher reference correlation values (0.6–0.9) had similar values during the visual attentional task. In the anticipatory attention paradigm, pairs of signals had similar correlation values in the reference state and during the attentional task. C and D. Scatterplots of the cross-correlation values for individual pairs of columns in the model with simulated attentional states: stimulus-driven (C) and anticipatory (D). The overall shapes of the scatterplots are in accordance with the experimental data. The distance (mm) between columns is marked by a color defined by the color bar located to the right of the panels. Small distance pairs (adjacent columns) exhibit the largest cross-correlations while more distant columns yield lower cross-correlations. E and F. Quantitative comparison of experimental and simulated cross-correlation values. Boxplots show the median together with the first and third quartile of the cross-correlations while the mean is marked with a diamond. Note that the overall trend in the means, medians and ranges are comparable in the simulated and experimental signals. Asterisks show significant differences between the attention and reference state ($p<0.05$).

4.3. *Beta oscillations*

Based on above results, we set the cortical input, I_C, to 320 Hz in order to simulate the beta band activity during top-down attention. The typical activity of the cells from a single column during a 1 s simulation is presented in Figure 5. Figure 5A shows the raster plot of the spike occurrences for all neurons in the column. The instantaneous firing rates are shown in Fig. 5B, while the simulated LFP signal is shown in Fig. 5C. The power spectrum of the LFP signal exhibited a clear peak in the beta band (~20 Hz; Fig. 5D, blue line). Analogous beta peaks are visible in the power spectra of the time series of E and I population firing rates (Fig. 5D, red and blue lines).

4.4. *Cross-correlations in vivo and in the model*

Experimental cross-correlations

In Fig. 6 A and B, spatial beta correlations observed experimentally during the stimulus-driven (n = 11) and anticipatory (n = 14) visual paradigm are plotted against the correlation values obtained in the reference state (auditory paradigm), for individual electrode pairs. It can be seen that in the SD paradigm, attentional modulation strongly attenuated (in comparison to those obtained in the reference state) the spatial correlations that were relatively weak (<0.6), while those that were relatively strong remained unchanged (Fig. 6A). In the Ant paradigm the spatial correlation values (even below 0.6) were similar to those in the reference state (Fig. 6B). Accordingly, the lower correlation values deviate downward from the diagonal in the SD experiment's scatterplot (Fig. 6A) but remain close to diagonal for the Ant paradigm (Fig. 6B).

Simulated cross-correlations

Fig. 6 C and D show the simulated cross-correlations of the beta signals from all available pairs (n = 120) of activities in spatially different cortical sites. The observed scatterplots are similar to those described above in the in vivo conditions. In the modeled SD paradigm the cross-correlation values deviated downward from the diagonal (Fig. 6C) and in the simulated Ant conditions they were located more closely to the diagonal (Fig. 6D). In Fig. 6 C and D, the correlation value for a given pair of columns is marked with a color corresponding to the distance between them. The distance color scale is shown to the right of

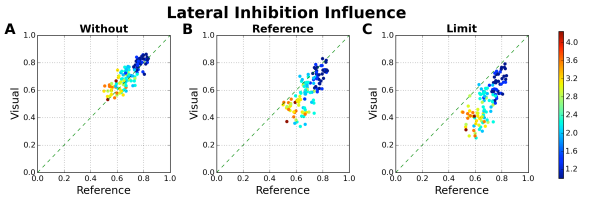

Fig. 7. Analysis of lateral inhibition strength of beta cross-correlations in the model. A and B. Cross-correlation values during the stimulus-driven (SD) attentional state are plotted against cross-correlation values in the reference state for individual pairs of columns in the model. A. Without lateral inhibitory connections, i.e., for W_{SL} = 0, cross-correlation values approximate the values obtained in the anticipatory attention paradigm. B. Reference SD conditions (same as in Fig. 6C). C. For strong lateral inhibitory connections (250% of reference value) cross-correlations further decrease and the scatterplot points deviate further away from the diagonal with respect to the correlations in the reference SD conditions (Fig. 7B). The color bar represents distance (mm) between the columns.

Fig. 6D. It can be seen that in general in both simulated attentional paradigms, the smaller the distance between the individual pairs of signals, the higher the correlation value between them (Fig. 6 C and D).

Comparison of mean cross-correlations

The box plots, which show the mean and range of the correlation values, confirm the differences between the correlations in the two paradigms. In the stimulus-driven attentional state the cross-correlation values had a lower mean value and a larger range than for reference state (Fig. 6E, Experiment). On the contrary, the mean value and range of the cross-correlations during the anticipatory attention task were similar to the values calculated during the reference condition (Fig. 6F, Experiment).

We performed statistical tests to estimate the significance of the observed differences in the correlation values between the attention and reference states in both paradigms. We used the paired Wilcoxon test since our data did not follow the normal distribution (Shapiro test, $p < 0.05$). In the experimental data the differences were significant only in the SD paradigm ($p < 0.05$). For 120 correlation pairs in the model, we observed that the differences in correlation were significant in both paradigms ($p<0.05$). However, the test performed is characterized by a higher statistical power than that used in experimental data, due to the different population sample sizes (120 in the model, compared to 11 for the SD and 14 for the Ant in experimental conditions). We, therefore, performed multiple statistical tests (1000) on randomly selected subpopulations, counting 11 (for SD) and 14 (for Ant) correlation values. Next, we computed the percentage of these tests for which the p-values were less than 0.05. In the modeled SD paradigm more than 97.5% of the random subpopulations resulted in p-values less than 0.05, confirming the results obtained with larger sample. On the other hand, for the Ant paradigm, only 17.7% of the random subpopulations resulted in a p-value less than 0.05. Based on these results we conclude that the modeled correlation differences between the attentional and reference states are in agreement with experimental results, which showed a significant effect in the SD paradigm but no significant differences in the Ant paradigm.

4.5. *Influence of lateral inhibition strength*

To provide further insight into role of lateral inhibition in shaping the model's beta correlations we performed additional simulations of the SD paradigm with different values of lateral inhibition strength, characterized by the weight (W_{SL}) of specific I_S input arriving at inhibitory cells in adjacent columns. The results are presented in Fig. 7. Without lateral inhibition, that is, for W_{SL} = 0 (Fig. 7A), the scatterplot of the cross-correlations is similar to that obtained for the Ant conditions (Fig. 6D). In reference conditions corresponding to SD paradigm (Fig. 7B) the cross-correlation values decreased and deviated downward from the diagonal. For strong lateral inhibition, with W_{SL} = 1.0, corresponding to the complete inhibition of activity in the surrounding regions, the cross-correlation values decreased even more and further deviated downward from the diagonal (Fig. 7C).

4.6. *Influence of center-surround organization on cross-correlations*

In order to better understand the observed general decrease in cross-correlations and the strong de-correlations of specific pairs in SD conditions (Fig. 6C) we analyzed the dependence of correlation values on spatial organization of the columns that were influenced by sensory input. We therefore divided the modeled network regions into different categories depending on their spatial relation to the stimuli. We defined the following: (i) stimulated (center) regions, which

received the specific excitatory visual input I_S from the thalamus, (ii) inhibited (surrounding) regions, which received lateral inhibitory inputs, and (iii) regions not related to the stimulus. Next, we analyzed how the cross-correlation values depended on associations of the

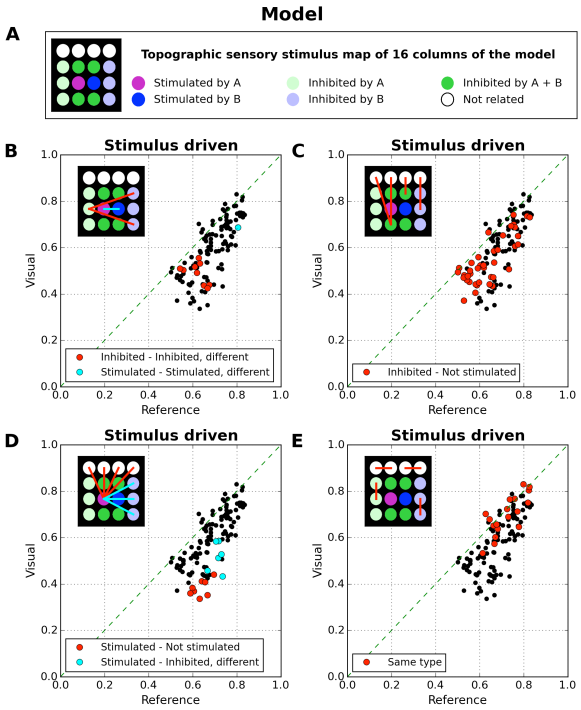

Fig. 8. Cross-correlations between individual pairs of columns in the model divided according to their spatial relation to the stimulation site. The different column categories are marked with different colors as indicated in topographic sensory stimulus map (A). Each scatterplot (B–E) shows the same data points, color points correspond to correlations between specific categories of columns indicated in the schematic topographical plot by color lines (inset); the remaining correlations are marked by black points. It can be seen that the correlations between the inhibited columns and between inhibited and non-related columns exhibit a moderate decrease (B and C). The strongest decrease is observed in correlations between the stimulated and not related columns (D). Correlations between columns of the same type – either inhibited or not related – remain largely unchanged (E).

involved columns with the same or different categories. The results of the analysis are shown in Fig. 8. The correlations of the columns that were excited or inhibited by different inputs are shown in Fig. 8B. It can be seen that the correlations between two columns belonging to different inhibitory surround regions exhibited a moderate decrease in the stimulus-driven condition (red points). A similar effect can be seen for two stimulated columns (light-blue point). A roughly similar decrease in correlations during SD vs. reference conditions was observed between inhibited and non-related columns (Fig. 8C). The strongest decrease was observed for correlations between stimulated and non-related columns (Fig. 8D, red points). Finally, correlations between columns of same type (inhibited by the same stimulus or not related) were mostly unaffected by the visual stimulus (Fig. 8E).

5. Discussion

The aim of the present study was to test, in a computational model, the neurophysiological hypothesis of the mechanism forming different beta activation maps in the primary visual cortex as observed in two distinct attentional tasks. In the experiment performed on cats[19] we have shown that the cross-correlation values of the beta frequency signals between spatially scattered cortical recording sites were similar during top-down attentional modulation (anticipatory attention) but were considerably different during bottom-up attentional modulation (stimulus-driven attention). We hypothesized that this effect may be explained by lateral inhibitory interactions activated by the process of attentive vision. In order to test this hypothesis we developed a large scale model of the cortical network that was composed of regular spiking, excitatory pyramidal cells, and fast spiking, inhibitory interneurons, with their connectivity based on available anatomical data. Using this model, we simulated three different activation states of the primary visual cortex that corresponded to the experimental tasks of auditory (reference) and visual (stimulus-driven and anticipatory) tasks. The model replicated the paradigm-specific beta activation maps that were dependent on the lateral inhibitory mechanism in accordance with the hypothesis. Additionally, we obtained a novel insight into the experimentally observed correlation patterns. Beta generation, spatial beta correlations, and new model predictions are discussed successively below.

5.1. *Beta generation mechanism*

For a wide range of external excitatory input rates (100 Hz – 3 kHz) the network generated LFP oscillations in a wide range of dominant frequencies spanning the beta/gamma range (Fig. 3A). To determine beta generation mechanism in the model, we performed simulations in the intact network and in modified

networks where connections between the cells were selectively removed (Fig. 4). The analysis showed that the emergence of oscillatory activity was mediated by reciprocal interactions between pyramidal cells and interneurons termed pyramidal-interneuron gamma (PING) mechanisms.[41] PING rhythms are generated with synchronous volleys of the excitatory population followed by inhibitory ones, as was also found in our model (Fig. 5B). The dominant oscillation period is strongly dependent on the strength of the external excitatory input (Fig. 3A), which controls the recovery time following inhibition in excitatory neurons. Although PING has been used to explain gamma, and sometimes also higher beta, rhythms, that is 20–80 Hz[42-45] frequency range, our modelling results suggest that this mechanism may also account for the lower beta frequencies below 20 Hz. It has been shown that in the cats stimulated by naturalistic video sequences, neurons in primary visual cortex fired mainly at low frequencies <5 Hz.[46] In our model firing rates below 5 Hz correspond to synchronized network oscillations below 20 Hz (Fig. 3B). In our cats attention experiments[2] the active beta range was 16-24 Hz. Accordingly, in the model we set the value of the external attentional input at 320 Hz for which a dominant peak about 20 Hz was observed in the LFP spectrum (Fig. 5D).

It can be noted (Fig. 5D) that at low frequencies the power spectrum of the modeled signals lacks the typical $1/f$ relation observed for spontaneous brain activity.[47, 48] It has been postulated that this phenomenon arises due to self-organized criticality[49] or due to the dendritic filtering of the Poisson spike trains.[50, 51] None of these processes has been implemented in our model and accordingly the spectra of the modeled signals did not exhibit this property. However, in both real and simulated signals we analyzed only rhythmic activities in the beta frequency range and therefore the exact shape of the background spectrum should not have influenced the results of cross-correlation analysis.

Another difference between experimental and our modeled LFP spectra is single dominant frequency in the model, while in the neocortex oscillations at different frequencies may coexist. It has been shown [52, 53] that different cortical rhythms differentially support feedback and feedforward processing in the visual system. Also it has been reported[54] that in the neocortical slices interaction between gamma ~40 Hz and beta2 ~25 Hz rhythms produced beta1 ~15 Hz rhythm by a process called concatenation. In our simulations we couldn't reproduce these results, as they require models with more realistic multilayered cortical architecture.

5.2. *Spatial beta correlations*

In the model we succeeded in reproducing the difference between the spatial beta correlation patterns observed experimentally during stimulus-driven and anticipatory attention tasks.[19] We posit that this difference could be attributed to the lateral inhibitory mechanism, which is activated by feed-forward inhibitory inputs during processing of the visual stimulus (bottom-up attention), but which remains inactive during stimulus anticipation (top down attention) in accordance with the organization of visual cortex circuitry.[7, 36] Accordingly, anticipatory attention results in uniform activation of cortical columns and homogenous pattern of inter-column. In contrast, stimulus-driven attention leads to an increased activation of the target columns and inhibition of neighboring columns. The resulting heterogeneity in the activation level across neighboring columns in the visual cortex increases the variability of the spatial cross-correlations. Additionally, the inhibited columns decrease internal activity and produce weaker correlations together with other columns. It leads to a decrease in the overall correlation level with respect to the reference state, as shown in Fig. 6E. We also show that increasing lateral inhibition strength to non-physiological values, when activity in inhibited columns is completely depressed, decreases the spatial cross-correlations even further (Fig. 7C). In contrast, when the lateral inhibition mechanism is removed (Fig. 7A) the cross-correlations patterns in the stimulus-driven and anticipatory paradigms are similar.

5.3. *Model predictions*

Beta cross-correlations depend on inter-columnar distance

We found that in the model, in both attentional paradigms the distance between the activated columns strongly determines cross-correlation values (Fig. 6C, D). In the model, this comes from the assumption that long-range inter-column excitatory connections reached only the neighboring columns. Such connectivity pattern mimicked the primary visual cortex, in which

connections from neurons more distant than 2 mm are significantly less common.[55] We therefore predict that a similar rule applies to experimental results, namely that the cross-correlation values depend on the distance between the activated columns. There is indirect evidence that supports this prediction. As shown earlier, the time lags of the correlograms were shorter for strongly correlated pairs and longer for weakly correlated ones.[19] Time lags might be directly related to the distances between columns and axonal conduction times. However, they may also depend on the strength of functional (not structural) connections. Hence our model's prediction remains to be tested experimentally.

Beta cross-correlations depend on sensory inputs arrangement

Additionally, we found that in the stimulus-driven condition, correlations that were high during the reference (auditory) task remained high, while those that initially had moderate or lower values, decreased even further during the stimulus-driven attention task (Fig. 6A). We were able to explain this effect in the model by dividing the columns into different categories according to their spatial relation to the stimuli (stimulated – central, inhibited – surrounding and not related). Our analysis showed that pairs of signals, which exhibited significant decrease in correlation during visual attention state, were those pairs that characterized activities in columns of different categories (e.g. center-surround, Fig. 8B-D). Columns that belonged to the same category (inhibited or not related) did not exhibit decreased correlation values during the SD condition (Fig. 8E). These modeling predictions might be tested experimentally. To this end, electrode locations could be divided into categories (activated, inhibited or not related) based on their behavior during the attentional stimulus-driven task in relation to the reference condition. Next, the beta cross-correlations of columns belonging to the same or to different categories might be evaluated. We suggest that such reciprocal interactions between the model and experiment are likely to provide additional insight into the origin and role of correlated beta activities during attentional tasks.

Acknowledgements

This research was carried out with the support of the Interdisciplinary Centre for Mathematical and Computational Modelling (ICM) University of Warsaw under grant no G57-3.

References

1. L. Leocani, C. Toro, P. Manganotti, P. Zhuang and M. Hallett, Event-related coherence and event-related desynchronization/synchronization in the 10 Hz and 20 Hz EEG during self- paced movements, *Electroencephalogr. Clin. Neurophysiol. - Evoked Potentials* **104** (1997) 199-206.
2. M. Bekisz and A. Wróbel, 20 Hz rhythm of activity in visual system of perceiving cat., *Acta Neurobiol. Exp.* **53** (1993) 175-182.
3. T. J. Buschman and E. K. Miller, Top-down versus bottom-up control of attention in the prefrontal and posterior parietal cortices, *Science* **315** (2007) 1860-1864.
4. Y. B. Saalmann, I. N. Pigarev and T. R. Vidyasagar, Neural mechanisms of visual attention: How top-down feedback highlights relevant locations, *Science* **316** (2007) 1612-1615.
5. C. A. Bosman, J. M. Schoffelen, N. Brunet, R. Oostenveld, A. M. Bastos, T. Womelsdorf, B. Rubehn, T. Stieglitz, P. De Weerd and P. Fries, Attentional stimulus selection through selective synchronization between monkey visual areas, *Neuron* **75** (2012) 875-888.
6. J. R. Iversen, B. H. Repp and A. D. Patel, Top-down control of rhythm perception modulates early auditory responses, *Ann. N. Y. Acad. Sci.* **1169** (2009) 58-73.
7. X.-J. Wang, Neurophysiological and Computational Principles of Cortical Rhythms in Cognition, *Physiol. Rev.* **90** (2010) 1195-1268.
8. G. Pfurtscheller, A. Stancák and C. Neuper, Post-movement beta synchronization. A correlate of an idling motor area?, *Electroencephalogr. Clin. Neurophysiol.* **98** (1996) 281-293.
9. A. Pogosyan, L. D. Gaynor, A. Eusebio and P. Brown, Boosting Cortical Activity at Beta-Band Frequencies Slows Movement in Humans, *Curr. Biol.* **19** (2009) 1637-1641.
10. F. Lopes Da Silva, EEG: Origin and measurement, in *EEG - fMRI: Physiological Basis, Technique, and Applications* (Springer-Verlag Berlin Heidelberg, 2010), pp. 19-38.
11. S. Haegens, V. Nacher, A. Hernandez, R. Luna, O. Jensen and R. Romo, Beta oscillations in the monkey sensorimotor network reflect somatosensory decision making, *PNAS* **108** (2011) 10708-10713.
12. T. H. Donner, M. Siegel, R. Oostenveld, P. Fries, M. Bauer and A. K. Engel, Population activity in the human dorsal pathway predicts the accuracy of visual motion detection., *J. Neurophysiol.* **98** (2007) 345-59.
13. B. Pesaran, M. J. Nelson and R. A. Andersen, Free choice activates a decision circuit between frontal and parietal cortex, *Nature* **453** (2008) 406-409.

14. S. Weiss and H. M. Mueller, "Too many betas do not spoil the broth": The role of beta brain oscillations in language processing, *Front. Psychol.* **3** (2012) 201.
15. T. J. Buschman, E. L. Denovellis, C. Diogo, D. Bullock and E. K. Miller, Synchronous Oscillatory Neural Ensembles for Rules in the Prefrontal Cortex, *Neuron* **76** (2012) 838-846.
16. A. K. Engel and P. Fries, Beta-band oscillations-signalling the status quo?, *Curr. Opin. Neurobiol.* **20** (2010) 156-165.
17. M. Bekisz and A. Wróbel, Attention-dependent coupling between beta activities recorded in the cat's thalamic and cortical representations of the central visual field., *Eur. J. Neurosci.* **17** (2003) 421-426.
18. A. Wróbel, A. Ghazaryan, M. Bekisz, W. Bogdan and J. Kamiński, Two streams of attention dependent beta activity in the striate recipient zone of cat's lateral posterior - pulvinar complex., *J. Neurosci.* **27** (2007) 2230-2240.
19. M. Bekisz, W. Bogdan, A. Ghazaryan, W. J. Waleszczyk, E. Kublik and A. Wróbel, The primary visual cortex is differentially modulated by stimulus-driven and top-down attention, *PLoS ONE* **11** (2016) e0145379.
20. W. S. Anderson, P. Kudela, J. Cho, G. K. Bergey and P. J. Franaszczuk, Studies of stimulus parameters for seizure disruption using neural network simulations, *Biol. Cyb.* **97** (2007) 173-194.
21. R. J. Douglas and K. A. C. Martin, Neuronal circuits of the neocortex, *Annu. Rev. Neurosci.* **27** (2004) 419-451.
22. H. Markram, The Blue Brain Project, *Nature Rev. Neurosci.* **7** (2006) 153-160.
23. J. Heinzle, P. König and R. F. Salazar, Modulation of synchrony without changes in firing rates, *Cogn. Neurodyn.* **1** (2007) 225-235.
24. M. Bazhenov, N. F. Rulkov and I. Timofeev, Effect of synaptic connectivity on long-range synchronization of fast cortical oscillations., *J. Neurophysiol.* **100** (2008) 1562-1575.
25. A. Bacci, J. R. Huguenard and D. A. Prince, Modulation of neocortical interneurons: extrinsic influences and exercises in self-control, *Trends Neurosci.* **28** (2005) 602-10.
26. M. W. Reimann, C. A. Anastassiou, R. Perin, S. L. Hill, H. Markram and C. Koch, A biophysically detailed model of neocortical local field potentials predicts the critical role of active membrane currents, *Neuron* **79** (2013) 375-90.
27. T. Binzegger, A Quantitative map of the circuit of cat primary visual cortex, *J. Neurosci.* **24** (2004) 8441-8453.
28. A. Stepanyants, L. M. Martinez, A. S. Ferecsko and Z. F. Kisvarday, The fractions of short- and long-range connections in the visual cortex, *PNAS* **106** (2009) 3555-3560.
29. P. C. Bush and T. J. Sejnowski, Models of Cortical Networks, in *The Cortical Neuron* (Oxford University Press, Inc., 2012).
30. X.-J. Wang, J. Tegner, C. Constantinidis and P. S. Goldman-Rakic, Division of labor among distinct subtypes of inhibitory neurons in a cortical microcircuit of working memory, *PNAS* **101** (2004) 1368-1373.
31. D. Ferster and S. Lindström, An intracellular analysis of geniculo-cortical connectivity in area 17 of the cat, *J. Physiol.* **342** (1983) 181-215.
32. R. Llinás, I. Z. Steinberg and K. Walton, Relationship between presynaptic calcium current and postsynaptic potential in squid giant synapse, *Biophys. J.* **33** (1981) 323-351.
33. V. Braitenberg and A. Schüz, *Anatomy of the Cortex*. (Springer-Verlag Berlin Heidelberg, 1991).
34. S. Leski, H. Lindén, T. Tetzlaff, K. H. Pettersen and G. T. Einevoll, Frequency dependence of signal power and spatial reach of the local field potential, *PLoS Comput. Biol.* **9** (2013) e1003137.
35. A. Destexhe, D. Contreras and M. Steriade, Mechanisms underlying the synchronizing action of corticothalamic feedback through inhibition of thalamic relay cells., *J. Neurophysiol.* **79** (1998) 999-1016.
36. S. Grossberg and M. Versace, Spikes, synchrony, and attentive learning by laminar thalamocortical circuits, *Brain Res.* **1218** (2008) 278-312.
37. U. Mitzdorf, Current source-density method and application in cat cerebral cortex: investigation of evoked potentials and EEG phenomena., *Physiol. Rev.* **65** (1985) 37-100.
38. P. L. Nunez and R. Srinivasan, *Electric Fields of the Brain: The neurophysics of EEG*. (Oxford University Press, 2006).
39. G. Buzsáki, C. A. Anastassiou and C. Koch, The origin of extracellular fields and currents-EEG, ECoG, LFP and spikes, *Nature Rev. Neurosci.* **13** (2012) 407-420.
40. M.-O. Gewaltig and M. Diesmann, NEST (NEural Simulation Tool), *Scholarpedia* **2** (2007) 1430.
41. M. A. Whittington, R. D. Traub, N. Kopell, B. Ermentrout and E. H. Buhl, Inhibition-based rhythms: Experimental and mathematical observations on network dynamics, *Int. J. Psychophysiol.* **38** (2000) 315-336.
42. R. D. Traub, M. a. Whittington, E. H. Buhl, J. G. Jefferys and H. J. Faulkner, On the mechanism of the gamma --> beta frequency shift in neuronal oscillations induced in rat hippocampal slices by tetanic stimulation., *J. Neurosci.* **19** (1999) 1088-1105.
43. C. Borgers, S. Epstein and N. J. Kopell, Background gamma rhythmicity and attention in cortical local circuits: A computational study, *PNAS* **102** (2005) 7002-7007.
44. P. Tiesinga and T. J. Sejnowski, Cortical Enlightenment: Are Attentional Gamma Oscillations Driven by ING or PING?, *Neuron* **63** (2009) 727-732.
45. D. Vierling-Claassen, J. A. Cardin, C. I. Moore and S. R. Jones, Computational Modeling of Distinct Neocortical Oscillations Driven by Cell-Type Selective Optogenetic Drive: Separable Resonant Circuits Controlled by Low-Threshold Spiking and Fast-Spiking Interneurons, *Front. Hum. Neurosci.* **4** (2010) 198.
46. R. Baddeley, L. F. Abbott, M. C. Booth, F. Sengpiel, T. Freeman, E. a. Wakeman and E. T. Rolls, Responses of neurons in primary and inferior temporal visual cortices to natural scenes., *Proc. Biol. Sci.* **264** (1997) 1775-1783.
47. W. S. Pritchard, The brain in fractal time: 1/f-like power spectrum scaling of the human electroencephalogram, *Int. J. Neurosci.* **66** (1992) 119-129.

48. W. J. Freeman, L. J. Rogers, M. D. Holmes and D. L. Silbergeld, Spatial spectral analysis of human electrocorticograms including the alpha and gamma bands, *J. Neurosci. Methods* **95** (2000) 111-121.
49. H. K. C. Bédard, and A. Destexhe, Does the 1/f frequency scaling of brain signals reflect self-organized critical states?, *Phys. Rev. Lett.* **97** (2006).
50. W. J. Freeman and J. Zhai, Simulated power spectral density (PSD) of background electrocorticogram (ECoG), *Cogn. Neurodyn.* **3** (2009) 97-103.
51. H. Lindén, K. H. Pettersen and G. T. Einevoll, Intrinsic dendritic filtering gives low-pass power spectra of local field potentials, *J. Comput. Neurosci.* **29** (2010) 423-444.
52. T. van Kerkoerle, M. W. Self, B. Dagnino, M. A. Gariel-Mathis, J. Poort, C. van der Togt and P. R. Roelfsema, Alpha and gamma oscillations characterize feedback and feedforward processing in monkey visual cortex, *PNAS* **111** (2014) 14332-41.
53. A. M. Bastos, J. Vezoli, C. A. Bosman, J. M. Schoffelen, R. Oostenveld, J. R. Dowdall, P. De Weerd, H. Kennedy and P. Fries, Visual areas exert feedforward and feedback influences through distinct frequency channels, *Neuron* **85** (2015) 390-401.
54. A. K. Roopun, M. A. Kramer, L. M. Carracedo, M. Kaiser, C. H. Davies, R. D. Traub, N. J. Kopell and M. A. Whittington, Period concatenation underlies interactions between gamma and beta rhythms in neocortex, *Front. Cell. Neurosci.* **2** (2008) 1.
55. W. H. Bosking, Y. Zhang, B. Schofield and D. Fitzpatrick, Orientation selectivity and the arrangement of horizontal connections in tree shrew striate cortex, *J. Neurosci.* **17** (1997) 2112-2127.